Fabrication of a Cellulolytic Enzyme Cocktail Immobilised on Magnetic Multi-walled Carbon Nanotubes: Catalytic Kinetics and Reusability

This work is licensed under a Creative Commons Attribution 4.0 International License

C. W. Low,[a] M. S. M. Annuar,[b,*] and S. Ibrahim[a,c]

[a]Institute of Ocean and Earth Sciences, Institute of Advanced Studies, Universiti Malaya, Kuala Lumpur, 50603, Malaysia

[b]Institute of Biological Sciences, Faculty of Science, Universiti Malaya, Kuala Lumpur, 50603, Malaysia

[c]Universiti Tenaga Nasional, Putrajaya Campus, Jalan IKRAM-UNITEN, 43000, Kajang, Selangor Malaysia

doi: https://doi.org/10.15255/CABEQ.2026.2537

Original scientific paper
Received: May 15, 2026
Accepted: October 5, 2026

An enzyme-immobilised magnetised multi-walled carbon nanotube composite (E-*m*MWCNT) was fabricated by acid oxidation of pristine MWCNT, Fe_3O_4 deposition, AEAPTMS silanisation, glutaraldehyde activation, and covalent immobilisation of the NS22257 enzyme cocktail (Novozymes A/S). Raman, FTIR, FESEM and VSM analyses supported stepwise assembly. Saturation magnetisation increased from 6.95 emu g^{-1} for pristine MWCNT to 46.7 emu g^{-1} for E-*m*MWCNT, with a remanence of 2.02 emu g^{-1} and coercivity of 2.07 G, indicating soft-magnetic behaviour suitable for rapid magnetic separation. The immobilised system performed best at pH 4.0, 55 °C and 200 rpm using carboxymethyl cellulose (CMC), a soluble model substrate for endoglucanase activity. The immobilisation yield was 80 %, the activity recovery was 39 %, and the activity yield was 48 %, giving a preparation of 1000 U g^{-1}. E-*m*MWCNT showed saturation kinetics, with apparent Michaelis–Menten parameters of K_m = 17.2 g L^{-1} and V_{max} = 0.36 g L^{-1} min^{-1}, against 12.9 g L^{-1} and 2.22 g L^{-1} min^{-1}, respectively, for the free enzyme, corresponding to an 8.2-fold increase in K_m/V_{max} attributed to external and internal transport limitations. A resistances-in-series treatment of the double-reciprocal plots separated intrinsic kinetics from external transport limitation, giving an effective liquid–solid volumetric mass-transfer coefficient of 0.016 min^{-1}. Over twelve consecutive reaction cycles with magnetic recovery, the preparation retained 91 % of its first-cycle yield at the fifth cycle and 55 % at the eighth cycle, giving 8.0 first-cycle batch equivalents from a single enzyme charge. The trade-off is therefore between single-pass rate and cumulative output per enzyme charge, and on this evidence, the latter favoured immobilisation.

Keywords
enzyme, immobilisation, multi-walled carbon nanotubes, magnetic, nanobiocatalyst

Introduction

Industrial enzyme-based catalytic systems are often limited by poor enzyme stability, the difficulty of recovering the catalyst, and the cost of single-use free enzymes. In hydrolytic applications, these limitations are even more significant because free enzymes disperse readily throughout the reaction medium, making them almost impossible to reuse. Immobilisation offers a practical route to improved enzyme handling, stability and operational lifespan. Conventional immobilisation matrices, however, often suffer from low surface area, weak structural integrity, enzyme leaching, or transport limitations that reduce catalytic effectiveness[1,2].

Nanomaterials have gained attention as immobilisation supports. Among them, multi-walled carbon nanotubes (MWCNTs) are especially promising, offering high surface area, mechanical strength, thermal resilience, and a surface that is readily functionalised chemically[3]. Surface oxidation and subsequent modifications introduce reactive groups, mainly carboxyl, hydroxyl, and carbonyl groups, which improve dispersion and allow enzymes to be attached covalently and stably. Consequently, MWCNTs have been adopted as enzyme scaffolds, and the same chemistry underpins their wider use as platforms for coupling biological molecules[4].

Nonetheless, recovering immobilised enzymes from liquid-phase reactions remains a significant operational challenge. Magnetisation of MWCNTs addresses this limitation where the catalyst can be

*Corresponding author: Professor Dr. Mohamad Suffian bin Mohamad Annuar, email: suffian_annuar@um.edu.my

pulled out of suspension using an external magnet, thereby minimising enzyme losses and simplifying downstream handling[5].

Previous studies have established magnetic carbon-based supports for enzyme immobilisation[6,7]. The commonly used functionalisation steps —acid oxidation, iron oxide co-precipitation, silanisation, and glutaraldehyde coupling—are themselves well established. The coupling chemistry has been reported for three antibody-attachment routes on carboxylated MWCNT in an electrochemical immunosensor, with the covalent route proving decisive for its performance[8]. Nevertheless, two aspects remain under-addressed. Firstly, reported magnetic MWCNT supports have been used almost exclusively for single purified enzymes, such as a single cellulase preparation[7] or a lipase[6], whereas immobilisation of a multi-component industrial cocktail raises a different problem. Components that differ in molecular mass, isoelectric point and surface lysine distribution all compete for a limited number of activated aldehyde sites, so the immobilised activity profile more often differs to that of the free preparation. Secondly, the increased apparent K_m usually reported for immobilised cellulolytic systems is routinely attributed to diffusional limitation, without separating transport from intrinsic kinetics or examining what that penalty yields in terms of repeated use of the same catalyst charge. Immobilisation may improve operational robustness, but it can also impose diffusional and steric constraints on substrate conversion[1,2]. The present work addresses these two gaps. It characterises the covalent assembly of an industrial cellulolytic cocktail on a magnetically recoverable MWCNT support, separates the external transport contribution to the kinetic penalty from intrinsic kinetics and quantifies it as a lumped mass-transfer coefficient, and evaluates the preparation across twelve consecutive reaction cycles. Nevertheless, activity measurement using a single model substrate is limited in its ability to distinguish how the individual cocktail components divide between the support and supernatant.

This study aimed to prepare a magnetically recoverable enzyme-immobilised MWCNT composite and to evaluate its physicochemical and catalytic properties. The composite, designated E-*m*MWCNT, was synthesised through sequential oxidation, magnetisation, silanisation, and covalent enzyme immobilisation. The preparation was characterised by Raman spectroscopy, Fourier-transform infrared spectroscopy (FTIR), field emission scanning electron microscopy (FESEM), and vibrating sample magnetometry (VSM), followed by reaction optimisation, kinetic evaluation and a twelve-cycle reuse study using carboxymethyl cellulose (CMC), a soluble model substrate for endoglucanase activity[9]. The substrate–velocity data were then analysed using a resistances-in-series treatment to separate intrinsic kinetics from external mass-transfer limitation.

Materials and methods

Materials

Multi-walled carbon nanotubes (MWCNTs; outer diameter 90–110 nm, purity > 95 %) were obtained from Sigma-Aldrich (Malaysia). Sulphuric acid (H_2SO_4, 95–98 %), nitric acid (HNO_3, 65 %), iron (II) sulphate heptahydrate ($FeSO_4·7H_2O$), iron (III) chloride ($FeCl_3$), sodium hydroxide (NaOH), ammonium hydroxide (NH_4OH, 25 %), and glutaraldehyde solution (50 %) were used for nanotube functionalisation, magnetisation and enzyme immobilisation. *N*-(2-aminoethyl)-3-aminopropyltrimethoxysilane (AEAPTMS) was used as the silanising agent. The commercial enzyme cocktail NS22257 (Novozymes A/S, Denmark), containing cellulase components together with β-glucosidase, hemicellulase and AA9 activities, was used for immobilisation and catalytic assays. Carboxymethyl cellulose sodium salt (CMC; CAS 9004-32-4, chemically pure grade, R&M Chemicals (Malaysia)) was used as the substrate for reaction optimisation and kinetic studies. All other chemicals were of analytical grade and used without further purification. Deionised water was used throughout the study.

Functionalisation of pristine MWCNTs

Pristine MWCNTs were oxidised to introduce oxygen-containing surface groups and improve dispersibility[10–12]. Briefly, 1.0 g of pristine MWCNTs was added to 100 mL of a concentrated acid mixture of H_2SO_4:HNO_3 (3:1, v/v) and stirred at 150 rpm for 3 h in a fume hood. After cooling to room temperature (25 ± 2 °C), the oxidised nanotubes were separated by centrifugation at 4000 rpm for 5 min and washed repeatedly with deionised water until the supernatant reached neutral pH. The recovered material was then dried at 60 °C overnight to obtain carboxylated MWCNTs (*c*-MWCNTs).

Magnetisation of *c*-MWCNTs

The *c*-MWCNTs were magnetised by *in situ* co-precipitation. $FeCl_3$ (0.54 g, 3.33 mmol) and $FeSO_4·7H_2O$ (0.28 g, 1.01 mmol) were dissolved in 100 mL of deionised water, giving a Fe^{3+}:Fe^{2+} molar ratio of 3.3:1. Iron (II) was therefore the limiting reagent, and the iron charge exceeded the 2:1 stoichiometry of magnetite. The co-precipitation route followed published procedures[13,14]. The solution was heated to 80 °C under continuous stirring at

200 rpm, after which 0.5 g of *c*-MWCNTs was gradually dispersed into the iron salt solution using an overhead stirrer to ensure uniform suspension. Once the mixture had stabilised at 80 °C, 2.5 M NH_4OH was added dropwise until the suspension reached pH 10, initiating the co-precipitation of iron oxide nanoparticles on the nanotube surface. The suspension was maintained at 80 °C for 1 h with constant stirring. After cooling to room temperature, the black precipitate was separated using a permanent magnet, washed repeatedly with deionised water until the decanted liquid reached neutral pH, and dried at 60 °C overnight to obtain magnetised MWCNTs (*m*MWCNTs).

Silanisation of *m*MWCNTs

To introduce amine groups for covalent enzyme attachment, the magnetised nanotubes were silanised with AEAPTMS[15]. Briefly, 0.5 g of *m*MWCNTs was dispersed in 50 mL ethanol:water mixture (95:5, v/v), followed by the addition of 2 % (v/v) AEAPTMS. The pH was adjusted to 3.5 using glacial acetic acid, and the suspension was shaken for 4 h at room temperature. The product was then magnetically collected, washed thoroughly with ethanol to remove unreacted silane, and dried at 60 °C overnight. This step produced amine-functionalised magnetic nanotubes (NH_2–*m*MWCNTs), which served as the support for enzyme immobilisation.

Enzyme immobilisation on amine-functionalised *m*MWCNTs

Enzyme immobilisation was carried out by covalently coupling the NS22257 enzyme cocktail (Novozymes A/S) to NH_2–*m*MWCNT, using glutaraldehyde as a bifunctional crosslinker[1,16]. The manufacturer describes the cocktail as comprising cellulase components boosted with proprietary activities, including AA9 (lytic polysaccharide monooxygenase), improved β-glucosidases and a range of hemicellulase activities. Endoglucanase activity within this blend is shown directly by the hydrolysis of CMC reported herein. The manufacturer quotes optimal performance at 50–55 °C and pH 4.75–5.25, measured using unwashed acid-pretreated corn stover at 18 % total solids over three to five days. The manufacturer also advises that the preparation contains a significant quantity of sugar; therefore, a blank should be run alongside the reaction. These figures are quoted as supplied and were not independently verified in the present study. Glutaraldehyde concentration was screened over 7.5–17.5 % (v/v) (Δ2.5 %), and each preparation was subjected to twelve consecutive reaction cycles as described further herein. The consistency in expressed activity per unit of immobilised activity was used to select the glutaraldehyde concentration, rather than first-cycle activity or absolute cumulative output, yielding 10.0 % (v/v) (see Table 1, Results and Discussion).

For surface activation, 0.5 g NH_2–*m*MWCNTs was suspended in 50 mL of 10.0 % (v/v) glutaraldehyde prepared in 0.05 M phosphate buffer (pH 7.0). The suspension was stirred gently at room temperature for 2 h to introduce reactive aldehyde groups on the carrier surface[16]. The activated support was then separated magnetically, washed thoroughly with phosphate buffer to remove excess glutaraldehyde, and re-suspended in 45 mL phosphate-buffered saline (PBS), pH 7.0.

For enzyme coupling, 0.1 g glutaraldehyde-activated *m*MWCNTs was suspended in NS22257 enzyme solution diluted fivefold, i.e., one part enzyme solution to four parts deionised water. Coupling was allowed to proceed for 12 h at room temperature with gentle shaking at 150 rpm. The immobilised enzyme preparation was magnetically separated and washed repeatedly with PBS (pH 7.0) to remove non-covalently bound enzyme. The washings from each round were assayed using the DNS method with CMC as substrate to confirm the absence of residual CMC-hydrolysing activity. Since this assay reports endoglucanase-type activity only, it excludes the assaying of β-glucosidase, hemicellulase or AA9 components in the washings. The resulting enzyme-immobilised magnetised MWCNT (E-*m*MWCNT) preparation was stored in PBS (pH 7.0) at 4 °C until further use.

Enzyme activity is expressed in units (U), where one unit is the amount of enzyme liberating 1 μmol of reducing sugar as glucose equivalents per minute under the assay conditions described herein.

Immobilisation performance was evaluated on an activity basis. The reaction rate of the enzyme stock offered to the support (A_i), of the residual supernatant after coupling (A_r), and of the recovered immobilised preparation (E_a) were each determined by DNS assay using CMC as the substrate, in triplicate, with a 5 min incubation. Four quantities were derived from these three rates: immobilisation yield = $(A_i - A_r)/A_i \cdot 100$ %; loss of activity on immobilisation = $(A_i - A_r - E_a)/A_i \cdot 100$ %; activity yield = $E_a/(A_i - A_r) \cdot 100$ %; and activity recovery = $E_a/A_i \cdot 100$ %. The immobilisation yield is the fraction of the offered activity that is no longer detected in solution after coupling. The loss of activity is the fraction that is neither detected in solution nor recovered on the support. The activity yield compares the recovered activity with the fraction removed from solution, while the activity recovery compares that same recovered activity with the activity originally offered. These four quantities are not independent. The loss of activity and activity recovery add up to the immobilisation yield, while the fractions of the offered activity that remain in solution, are lost, or are recovered together, account for 100 %.

A protein loading parameter was not determined. The composition of NS22257 is not disclosed in the manufacturer's data sheet; therefore, a total protein content could not be apportioned among the cocktail components or attributed to the endoglucanase activity measured here. Furthermore, the manufacturer advises that the preparation contains a significant quantity of sugar, which interferes with copper-reduction-based protein assays, while dye-binding assays are unreliable for a black carbon carrier bearing surface amine groups.

In this study, both free and immobilised enzyme preparations were standardised at 100 U; hence, all comparisons were made on an equal-activity basis.

Characterisation of E-*m*MWCNTs

The materials obtained after oxidation, magnetisation, silanisation, glutaraldehyde activation, and enzyme immobilisation were characterised to confirm the structural, chemical, morphological, and magnetic changes using field emission scanning electron microscopy (FESEM), Fourier-transform infrared spectroscopy (FTIR), Raman spectroscopy, and vibrating sample magnetometry (VSM), respectively. Not every technique was applied to every stage, e.g., FESEM covered the pristine, carboxylated, magnetized, silanised, glutaraldehyde-activated, and enzyme-immobilised materials; Raman analysis compares the pristine and magnetised materials; and VSM compares the pristine MWCNTs material with E-*m*MWCNTs.

FESEM imaging

Field emission scanning electron microscopy was performed using an FEI Quanta FEG 650 S instrument (FEI Company, USA). Dried powder samples were mounted on conductive carbon tape fixed to aluminium stubs. The samples were then examined for surface morphology and structural changes across the successive stages of functionalisation and immobilisation.

For morphological comparison, FESEM images were obtained at magnifications of 500×, 5,000×, 50,000×, and 100,000× to assess dispersion, surface uniformity, and the visible changes that accompanied stepwise functionalisation and enzyme coupling.

FTIR spectroscopy

FTIR analysis was carried out using a Perkin Elmer Spectrum 400 spectrometer (USA) equipped with an attenuated total reflectance (ATR) accessory with a diamond crystal. Samples were analysed directly in solid form, and spectra were recorded over a wavenumber range of 4000–450 cm^{-1} against a background spectrum. FTIR was used to identify surface functional groups and to confirm the chemical changes at each stage of MWCNT functionalisation and enzyme immobilisation.

Raman spectroscopy

Raman spectroscopy was performed using a Renishaw inVia Raman Microscope (Renishaw plc, UK). Solid samples were placed on a clean sample holder and focused under the microscope before spectral acquisition. Multiple scans were collected to improve signal quality, and the spectra were read mainly for the characteristic *D* and *G* bands of carbon materials, together with the extra peaks that appear when iron oxide is deposited during magnetisation.

Vibrating sample magnetometer

Magnetic characterisation was conducted using a Lake Shore 7400 Series Vibrating Sample Magnetometer (VSM). Powder samples were weighed, mounted in a non-magnetic holder and centred in the instrument before measurement to ensure a reliable signal. VSM was used to establish the magnetic behaviour of the magnetised and functionalised MWCNT samples, and to confirm whether they were receptive to magnetic stimulus.

Determination of optimal catalytic conditions

Reaction optimisation of the E-*m*MWCNT preparation was performed using CMC as the substrate at an initial concentration of 5 g L^{-1}. This concentration balanced two requirements: an excess of substrate for a 10-min assay, and a sufficiently low viscosity to minimise the likelihood that mixing would become rate-limiting. The effects of pH, temperature, and agitation were investigated separately.

Effect of pH on E-*m*MWCNT

A 50 mL CMC solution, prepared in deionised water and adjusted to the stated pH with 0.1 M citric acid or 0.1 M NaOH, without added buffer, was placed in a 150 mL beaker and incubated for 10 min at 50 °C with agitation at 200 rpm. The pH values tested ranged from 3.5 – 5.5 (ΔpH 0.5). The lack of a buffering system is a limitation, since the pH may drift as reducing sugars accumulate. An E-*m*MWCNT loading at 100 U was used in each assay. The reaction vessel was placed in a water bath and mixed using an overhead stirrer. All experiments were performed in triplicate. Reducing sugar was measured by the DNS assay[17] and the background subtracted, giving the net production used for rate and yield calculations.

Effect of temperature on E-*m*MWCNT

The same assay configuration and settings were used, with temperature varied from 40 to 75 °C (ΔT 5 °C) at pH 4.0.

Effect of agitation on E-*m*MWCNT

Agitation speed was varied from 100 to 500 rpm (Δ100 rpm) at pH 4.0 and 55 °C. Free-enzyme optima were determined in parallel with immobilised preparation over pH 2.0–7.0, 20–70 °C and 100–500 rpm. It was found that for agitation variable, free-enzyme yield varied by only 3.5 % across the 100–500 rpm range. Nevertheless, 200 rpm was selected for both free and immobilised enzyme preparations so that they could be compared directly.

Kinetic evaluation of the E-*m*MWCNT

The kinetic behaviour of E-*m*MWCNT was evaluated using CMC as the substrate at pH 4.0, 55 °C, and 200 rpm for 10 min, with 100 U of E-*m*MWCNT in a total reaction volume of 50 mL. CMC concentrations of 5 – 30 g L^{-1} (Δ5 g L^{-1}) were used to obtain the substrate-velocity data. The concentration range was selected in preliminary experiments to encompass the apparent K_m of the immobilised preparation and reach its saturation plateau; it was then extended to 30 g L^{-1} to investigate the onset of viscosity-limited behaviour. A loading of 0.1 g E-*m*MWCNT, corresponding to 100 U, was used in each assay. The Michaelis–Menten model was fitted to the data over the range 5 – 25 g L^{-1}. The 30 g L^{-1} point was measured but excluded from the fit because the velocity was lower than that at 25 g L^{-1}, and therefore fell outside the domain of a saturation model. The possible reasons for this decline are discussed in the Discussion section. The reducing sugar released was quantified using the DNS assay, and the velocity (V_0), defined as the mean reaction rate over the 10-min incubation period, was calculated from the net amount of reducing sugar produced. The apparent Michaelis constant (K_m) and maximum velocity (V_{max}) were estimated by fitting the data to the Michaelis–Menten model using GraphPad Prism 10 software.

Kinetic evaluation of the free enzyme

The kinetic behaviour of the free NS22257 enzyme cocktail was evaluated using CMC as the substrate under its optimised operating conditions. Reactions were carried out at 50 °C, pH 5.0, and 200 rpm for 10 min. CMC solutions were prepared in deionised water at concentrations of 2 – 15 g L^{-1}. The substrate concentration ranges for the two enzyme preparations differed because each range was selected to encompass the measured K_m of the respective preparation and reach its saturation plateau. The ranges overlapped between 5 and 15 g L^{-1}. Each reaction mixture had a total volume of 50 mL and contained free enzyme at 100 U.

At the end of the incubation, 1 mL aliquots were withdrawn and heated in a boiling water bath for 5 min to stop the reaction. Velocity (V_0), defined as the mean reaction rate over the 10-min incubation period, was calculated from the net amount of reducing sugar produced, and K_m and V_{max} were estimated by fitting the data to the Michaelis–Menten model using GraphPad Prism 10 software.

Analysis of external mass-transfer limitation

The double-reciprocal plot of the immobilised preparation was curved, whereas that for the free enzyme was linear. This curvature indicated that the observed reaction rate was influenced partly by the rate at which substrate was transferred from the bulk solution to the catalyst, rather than being determined solely by the intrinsic reaction kinetics. The data were therefore analysed using a resistances-in-series treatment, a standard approach for analysing immobilised enzymes under external film control[18,19]. The treatment describes two sequential steps: substrate is transferred across the thin liquid film surrounding each catalyst particle and then reacts at the particle surface. At steady state, both steps proceed at the same rate, which is the rate measured experimentally.

The transport step is described by:

$$v = k_L a\left([S]^b - [S]^s\right) \tag{1}$$

where $[S]^b$ and $[S]^s$ are the bulk and catalyst-surface substrate concentrations, respectively, and $k_L a$ is the effective liquid–solid volumetric mass-transfer coefficient. The intrinsic reaction follows Michaelis–Menten kinetics in terms of the surface concentration:

$$v = \frac{V_{max}[S]^s}{K_m + [S]^s} \tag{2}$$

The surface concentration cannot be measured, so it is eliminated between the two equations. Where $[S]^s$ is well below K_m, equation (2) becomes first order, $v = (V_{max}/K_m)[S]^s$, which rearranges to $[S]^s = v\,K_m/V_{max}$. Substituting this into equation (1) and collecting terms gives:

$$\frac{1}{v} = \left(\frac{1}{k_L a} + \frac{K_m}{V_{max}}\right)\cdot\frac{1}{[S]^b} \tag{3}$$

Equation (3) forms the basis of analysis. It shows that the slope of a double-reciprocal plot is simply the sum of two contributions: the intrinsic kinetic slope K_m/V_{max}, which belongs to the enzyme, and $1/(k_L a)$, which belongs to the transport step.

The transport coefficient is simply the reciprocal of the gap between the observed slope and the intrinsic slope:

$$k_L a = \frac{1}{\text{slope}_{\text{observed}} - \text{slope}_{\text{intrinsic}}} \quad (4)$$

The difference in slope of a double-reciprocal plot gives $k_L a$ (min^{-1}).

Internal transport within the network was not modelled separately; therefore, any internal contribution is included in the fitted value. The result is therefore an effective coefficient rather than a purely external one.

Repeated operational use of E-*m*MWCNT

Repeated operational use of E-*m*MWCNT was assessed by putting each immobilised preparation through twelve consecutive 10-min reaction cycles under the optimised conditions (5 g L^{-1} CMC, pH 4.0, 55 °C, 200 rpm). After each cycle, the preparation was recovered with a permanent magnet, washed with PBS to remove product and residual substrate, and resuspended in fresh substrate. The amount of reducing sugar released in each cycle was determined by the DNS assay, and yields are reported relative to the first cycle of the same preparation.

The same protocol was used for the glutaraldehyde concentration screen, so that cross-linker concentration was selected based on sustained performance across cycles rather than on first-cycle activity alone.

Data analysis

All experiments were performed in triplicate, and results are presented as mean ± standard deviation. Differences between treatment means were assessed using one-way analysis of variance (ANOVA) with Tukey's post-hoc test, taking significance at $p < 0.05$. All kinetic and repeated operational use plots include error bars showing the standard deviation of triplicate determinations, and kinetic parameters are reported with the 95 % confidence intervals obtained from the nonlinear fit in GraphPad Prism 10 software.

Results and discussion

Fabrication of E-*m*MWCNT

E-*m*MWCNT was fabricated sequentially, i.e., by acid oxidation of pristine MWCNTs, Fe_3O_4 deposition, AEAPTMS silanisation, glutaraldehyde activation, and covalent immobilisation of the NS22257 enzyme cocktail. Together, these steps yielded a magnetically recoverable, enzyme-immobilised composite, whose assembly was subsequently characterised using Raman spectroscopy, vibrating sample magnetometry, FTIR spectroscopy, and FESEM.

Raman analysis

Raman spectroscopy was used to investigate structural changes in the MWCNTs following acid functionalisation and magnetisation. Pristine MWCNTs exhibited the characteristic *D* and *G* bands associated with disordered and graphitic carbon, respectively. After magnetisation, additional peaks were observed at approximately 342, 482, and 678 cm^{-1} (Fig. S1, Supplementary Material), which were absent from the pristine samples. These peaks are consistent with a spinel iron oxide phase on the nanotube surface. Reference peak positions are 310, 554 and 672 cm^{-1} for magnetite and 365, 511 and 700 cm^{-1} for maghemite, with positions shifting depending on particle size and acquisition conditions[20,21]. Magnetite is also readily oxidised under the probe beam; therefore, the two phases were not distinguished here, and the assignment was made at the level of the spinel phase. The iron charge used here also exceeded the 2:1 Fe^{3+}:Fe^{2+} stoichiometry of magnetite; therefore, a partially oxidised, Fe^{3+}-rich spinel is expected following synthesis. The new signals provide spectroscopic evidence that the MWCNTs were modified as intended, while the main carbon bands remained evident, indicating that the nanotube backbone remained intact during the magnetisation step. The iron oxide signals confirmed that an iron oxide phase was deposited without disrupting the graphitic structure of the support. Magnetic functionality was thus introduced without compromising the carbon framework required for the subsequent silanisation and enzyme coupling steps.

VSM magnetic characterisation

The magnetic properties of the composites were measured using vibrating sample magnetometry to confirm the incorporation of an iron oxide phase and to determine whether the material could be recovered magnetically. Pristine MWCNTs exhibited relatively low magnetisation, with a saturation magnetisation of 6.95 emu g^{-1}, whereas the freshly prepared E-*m*MWCNT exhibited a saturation magnetisation of 46.7 emu g^{-1}. The enzyme-immobilised composite also exhibited a remanence of 2.02 emu g^{-1} and a coercivity of 2.07 G, indicating soft-magnetic behaviour suitable for rapid magnetic separation[5,21]. Fig. 1 shows the magnetic profiles of pristine MWCNTs and E-*m*MWCNT.

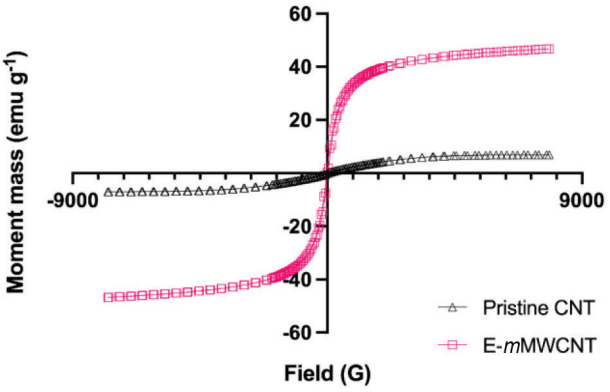


Fig. 1 – *Magnetometric profiles of pristine MWCNT and E-mMWCNT samples*

The substantial increase in saturation magnetisation confirmed that magnetic particles were successfully deposited on the nanotube framework. E-*m*MWCNT was expected to exhibit lower magnetisation than bare magnetic nanoparticles because neither the nanotubes nor the enzyme were magnetic; nevertheless, the value measured here was sufficiently high to enable magnetic recovery of the composite[5].

FTIR spectroscopy

FTIR spectra recorded after each modification stage showed progressive changes in surface chemistry. The spectra were interpreted in terms of the transitions associated with each stage of the assembly, and the complete peak assignments for all stages are given in Table S1 and Figs. S2–S5 (Supplementary Material). The oxidised, magnetised material shows a broad O–H stretching signal band at 3352.5 cm^{-1}, assigned to hydroxyl groups and adsorbed water on the oxidised carbon surface; a band in this region is present at all subsequent stages. No discrete carboxyl C=O band was resolved near 1700 cm^{-1} at any stage; therefore, carboxylation was not confirmed directly by these spectra. An Fe–O stretching band appears at 554.8 cm^{-1} and persists through silanisation (557.1 cm^{-1}), glutaraldehyde activation (555.5 cm^{-1}), and enzyme coupling (538.8 cm^{-1}), showing that the magnetic core endured subsequent steps. Since the infrared analysis started with the already oxidised and magnetised material, it recorded the persistence of that core rather than its deposition; deposition itself was established by the Raman spectra and the increase in saturation magnetisation. Silanisation was indicated by a strong Si–O–Si/Si–O–C band at approximately 1050 cm^{-1}, which was absent before AEAPTMS treatment[15,22]. A strong band at 1634 cm^{-1}, together with O–H/N–H stretching at 3281 cm^{-1}, is present in the enzyme-coupled preparation and is consistent with the presence of protein on the silanised magnetic support[16]. However, this band alone is not diagnostic of immobilised enzyme. A band of comparable magnitude was observed at 1631 cm^{-1} in the glutaraldehyde-activated support before enzyme introduction (Table S1, Supplementary Material), where the imine formed with the AEAPTMS amine absorbs in the same region. Moreover, no amide II band was observed in any spectrum. Enzyme immobilisation is therefore established here by the activity balance and subsequently supported by the twelve-cycle reuse series and FESEM micrographs, rather than by the infrared spectra alone.

Taken as a whole, the spectra support stepwise assembly of E-*m*MWCNT. The Fe–O band was preserved throughout the modification sequence, indicating that the magnetic core withstood the successive treatment steps, while the observed Si–O signals provided clear evidence of AEAPTMS grafting. The enzyme-bearing samples differed from the glutaraldehyde-cross-linked intermediate mainly in the silicon–oxygen region, and the infrared spectra did not, by themselves, distinguish immobilised protein from the cross-linked support. Considered together with the activity balance, the E-*m*MWCNT reusability study, and the other physicochemical analyses, the results are nevertheless consistent with the formation of an enzyme-immobilised, magnetically recoverable MWCNT composite.

FESEM microscopy

FESEM imaging showed the progressive surface changes across the functionalisation sequence, while the overall nanotube framework appeared preserved. At low and intermediate magnifications, pristine MWCNTs appeared as dense, compact aggregates with relatively smooth surfaces, whereas the acid-oxidised sample showed a more open, rougher, and more irregular network, consistent with oxidative etching. After AEAPTMS treatment and glutaraldehyde cross-linking, the nanotubes appeared more coated and condensed, with closer contact between adjacent fibres. The progressive changes according to the modification sequence are presented in Fig. 2.

The magnetised intermediate (*m*MWCNTs) was not imaged because the iron oxide phase interfered with electron-beam stability and image resolution on the instrument used. Iron oxide deposition was therefore confirmed by the Raman spectra and the increase in saturation magnetisation rather than by direct imaging.

At higher magnification, these differences became more distinct. The oxidised nanotubes appeared roughened and frayed compared with the pristine material, whereas the glutaraldehyde-treated samples exhibited more compact inter-fibre regions. The final enzyme-immobilised samples car-

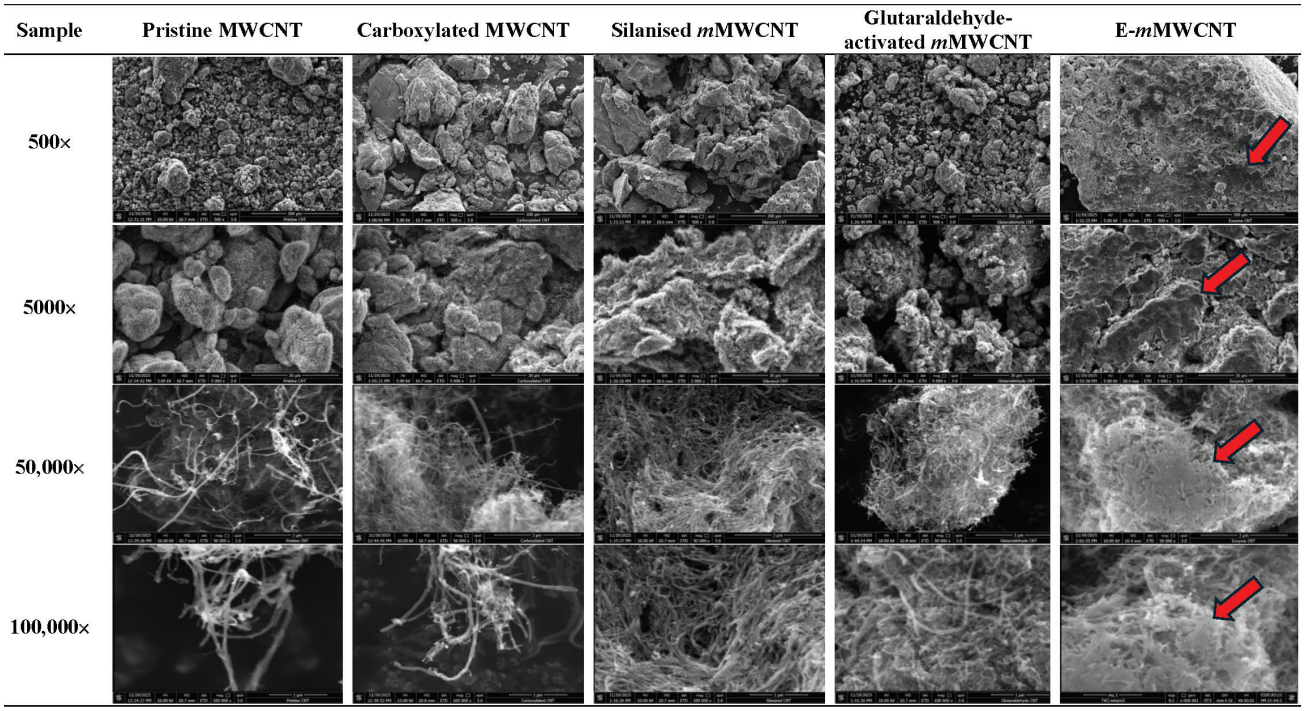


Fig. 2 – *Morphologies of MWCNTs with successive modifications*

ried distinct surface deposits and textured coatings, consistent with enzyme attachment to the modified nanotube network (red arrows). Overall, the FE-SEM images support stepwise surface modification and enzyme immobilisation without apparent loss of the tubular structure of the MWCNT platform.

Optimisation of reaction conditions

Optimization was carried out at an equivalent enzyme activity of 100 U for both the free enzyme and the E-*m*MWCNT preparations. Since NS22257 is a multi-component preparation and CMC is a soluble cellulose derivative hydrolysed by endoglucanase (EC 3.2.1.4), the reducing sugar released under these assay conditions is attributed predominantly to the endoglucanase activity of the blend. The remaining fraction, such as β-glucosidase, acts on cellobiose and short cello-oligosaccharides and contribute little directly to reducing-sugar release from CMC, although it may act on oligosaccharides generated by endoglucanase. Hemicellulase activity was not expected to act on CMC. AA9 activity requires an external electron donor, which was not supplied, and prefers crystalline to soluble substrate; therefore, its contribution here was negligible. This study therefore specifically characterises the immobilisation of endoglucanase activity.

Effect of pH

The hydrolytic performance of E-*m*MWCNT was measured over pH 3.5–5.5 using CMC as substrate (Fig. 3(a)). The highest reducing sugar yield, 1.6 ± 0.0 g L^{-1}, was obtained at pH 4.0, indicating that the immobilised system performed best under mildly acidic conditions. A lower yield was observed at pH 4.5 (1.2 g L^{-1}), whereas activity declined sharply at pH ≥ 5.0, with little or no detectable reducing sugar at higher values. No hydrolysis was detected at pH 3.5 either. Measurable activity was therefore confined to pH 4.0 and 4.5, indicating that the preparation operated within a narrow pH window rather than across a broad acidic range. ANOVA across the five pH levels confirmed the effect of pH, $F(4, 10) = 2021$, $p < 0.001$, and Tukey's HSD test distinguished pH 4.0 from pH 4.5 and both from the three inactive levels. The free enzyme, assayed under similar conditions, had an optimum at pH 5.0; thus, immobilisation shifted the optimum by one pH unit towards more acidic conditions, possibly due to alteration of the local microenvironment by the charged support surface[23].

The free enzyme was assayed in parallel over pH 2.0–7.0 (Fig. 3(b)). Measurable activity was confined to pH 3.0–6.0, with no reducing sugar detected at either pH 2.0 or pH 7.0. The optimum was pH 5.0, at which 11.7 ± 0.1 g L^{-1} reducing sugar was released, and activity declined sharply on either side of the optimum: pH 4.0 gave 4.0 ± 0.3 g L^{-1}, corresponding to 34 % of the peak value, while both pH 3.0 and pH 6.0 gave 3.1 g L^{-1} (27 %). ANOVA across the six pH levels confirmed the effect of pH, $F(5, 12) = 1237$, $p < 0.001$, and Tukey's HSD test placed pH 5.0 above every other level. As

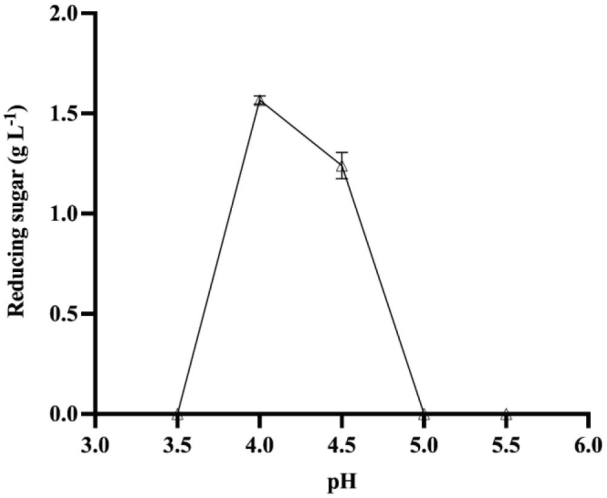


Fig. 3(a) – *pH profile of E-mMWCNT using CMC as substrate for hydrolysis*

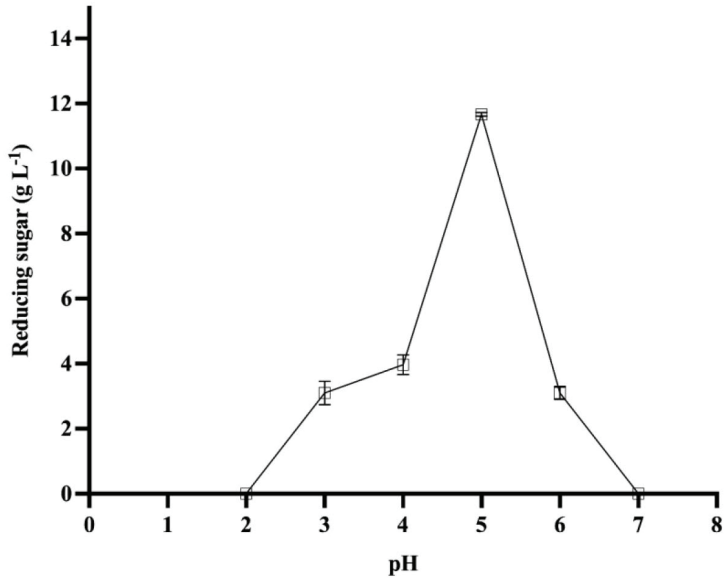


Fig. 3(b) – *pH profile of free-enzyme using CMC as substrate for hydrolysis*

with the immobilised preparation, two levels returned no detectable product and therefore had no variance. The decline around the optimum was not symmetric. On the acidic side, activity persisted over three pH units, falling to 34 % of the peak value at pH 4.0 and 27 % at pH 3.0 before disappearing at pH 2.0, whereas on the alkaline side, it fell to 27 % within a single pH unit and to zero at pH 7.0.

The free enzyme retained measurable activity across at least three pH units, whereas the immobilised preparation was active only at pH 4.0 and 4.5. Thus, immobilisation narrowed the practical pH window as well as shifted it towards more acidic conditions.

Effect of temperature

Temperature strongly affected the activity of E-*m*MWCNT. No hydrolysis was detected at 40 °C. The reducing sugar yield then increased from 0.03 g L^{-1} at 45 °C to 0.5 ± 0.0 g L^{-1} at 50 °C and reached a maximum of 1.2 ± 0.0 g L^{-1} at 55 °C, before declining sharply at higher temperatures. The yield decreased to 0.4 g L^{-1} at 60 °C, remained at 0.4 g L^{-1} at 65 °C, and decreased further to 0.3 g L^{-1} at 70 °C, with complete loss of detectable activity at 75 °C. The optimum operating temperature for the immobilised system was therefore 55 °C (Fig. 4(a)). ANOVA across the eight temperatures confirmed the effect of temperature, $F(7, 16) = 3401$, $p < 0.001$, and Tukey's HSD test placed 55 °C significantly above every other level. The yield at 50 °C was 2.5-fold lower, whereas only the 60 and 65 °C levels could not be separated from one another. The optimum of the immobilised preparation was 5 °C higher than that of the free enzyme, whose optimum of 50 °C was determined under the same assay conditions. This observation is consistent with conformational stabilisation on covalent attachment[24]. Both optima fall within the 50–55 °C range specified by the manufacturer for the free preparation.

The free enzyme was assayed over 20–70 °C in 10 °C increments (Fig. 4(b)). No hydrolysis was detected at 20 °C or 70 °C. The yield increased from 2.9 ± 0.1 g L^{-1} at 30 °C to 4.7 g L^{-1} at 40 °C, and reached a maximum of 5.3 ± 0.1 g L^{-1} at 50 °C, before declining to 2.4 ± 0.1 g L^{-1} at 60 °C. ANOVA confirmed the effect of temperature, $F(5, 12) = 3905$, $p < 0.001$, and Tukey's HSD separated every pair of temperatures except the two inactive levels, placing 50 °C above 40 °C at $p < 0.001$. The profile is broad below the optimum, with 40 °C still returning 89 % of the peak yield but declined rapidly above the optimum to 45 % at 60 °C and to zero at 70 °C. Comparison with the immobilised preparation is confined to the upper temperature range. At 60 °C, the free enzyme retained a greater proportion of its own optimum activity than E-*m*MWCNT, at 45 % versus 33 %. At 70 °C, the only temperature above 60 °C at which both preparations were assayed, this relationship was reversed: the free enzyme released no detectable product, while E-*m*MWCNT still yielded 0.3 g L^{-1}, corresponding to 21 % of its own optimum yield; product was undetectable only at 75 °C.

Effect of agitation speed

Agitation speed was examined over the range 100–500 rpm at the optimised pH and temperature (Fig. 5(a)). Yield increased from 0.7 ± 0.0 g L^{-1} at 100 rpm to 1.0 ± 0.0 g L^{-1} at 200 rpm and did not increase thereafter. Across the five speeds, ANOVA gave $F(4, 10) = 181$, $p < 0.001$, with Tukey's HSD test separating 100 rpm from every higher speed, while no pairwise differences were observed in the range 200–500 rpm. An analysis restricted to 200–

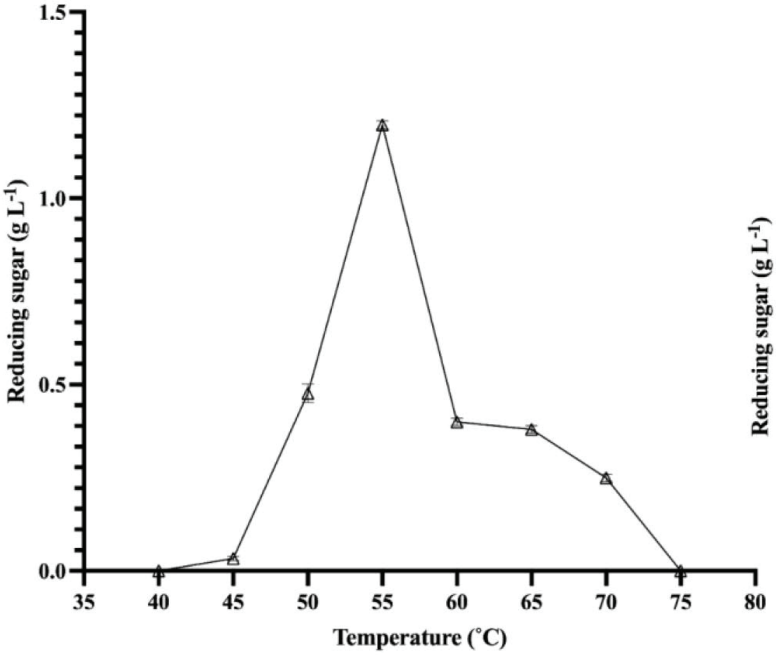


Fig. 4(a) – *Temperature profile of E-mMWCNT using CMC as substrate for hydrolysis*

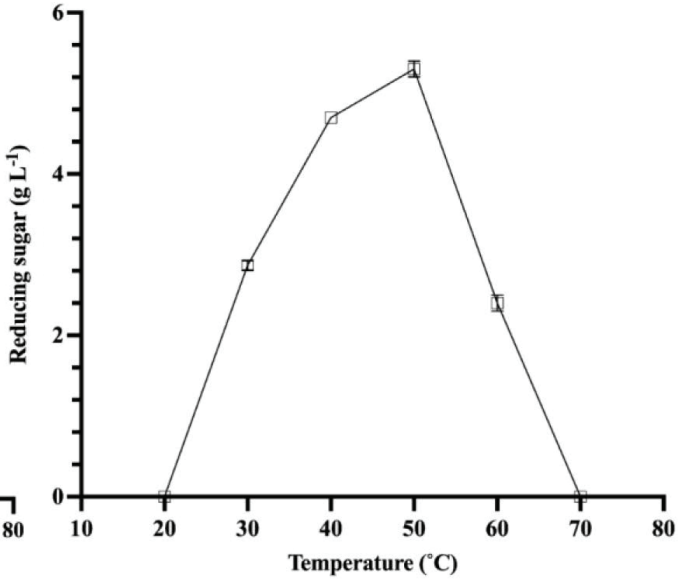


Fig. 4(b) – *Temperature profile of free-enzyme using CMC as substrate for hydrolysis*

500 rpm returned $F(3, 8) = 0.73$, $p = 0.56$, consistent with a plateau across which the yields varied by only 0.8 %. The next highest agitation rate, i.e., 200 rpm, was therefore selected as the operating speed, providing sufficient mixing duty to overcome the possible limitation observed at 100 rpm without an observable adverse effect of shear stress on the preparation.

The free enzyme behaved differently under the same treatment (Fig. 5(b)). Its yield was 4.7 ± 0.0 g L^{-1} at 100 rpm, decreased slightly to 4.6 ± 0.1 g L^{-1} at 200 rpm, and then increased slightly to 4.8 ± 0.0 g L^{-1} at 500 rpm. The yields across the entire range varied by 3.5 % relative to the lowest value. The lowest value occurred in the middle of the range rather than at the lowest speed, while the 100 rpm point was within 1.5 % of the maximum. The variation reached significance ($F(4, 10) = 4.92$, $p = 0.019$); however, Tukey's HSD test distinguished only the 200 and 500 rpm levels ($p = 0.014$), with all other pairwise comparisons returning $p \geq 0.085$.

The 26 % increase in yield when the agitation speed was raised from 100 to 200 rpm was therefore specific to the immobilised preparation. This

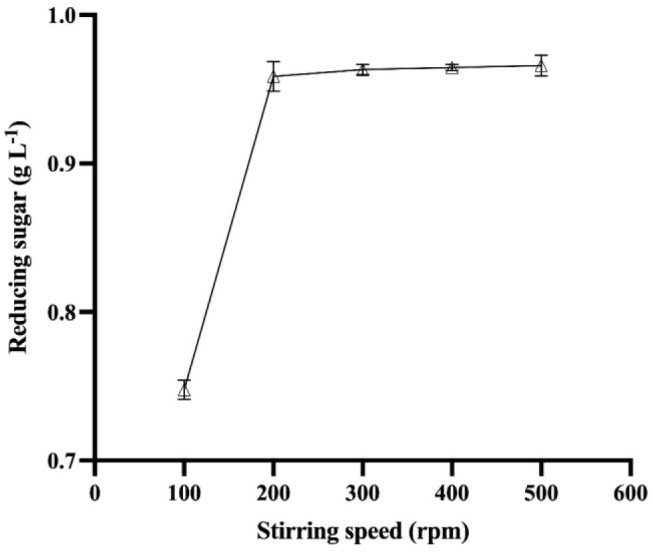


Fig. 5(a) – *Agitation speed profile of E-mMWCNT using CMC as substrate for hydrolysis*

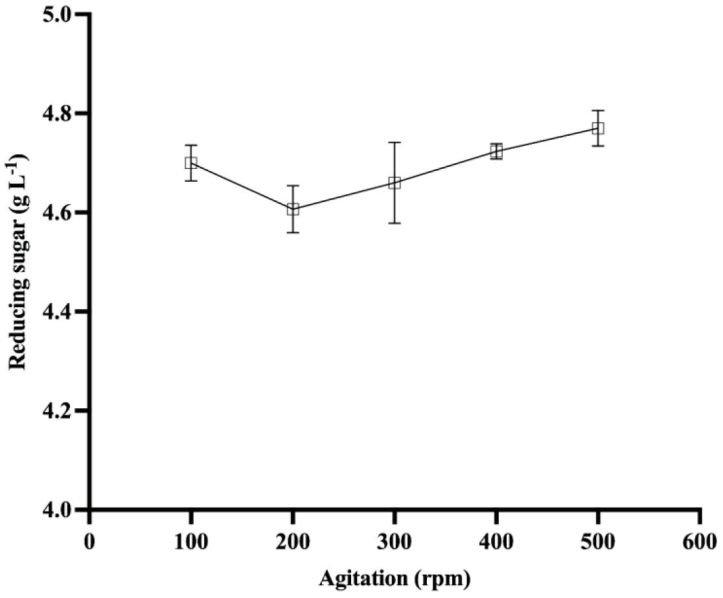


Fig. 5(b) – *Agitation speed profile of free-enzyme using CMC as substrate for hydrolysis*

Table 1 – *Immobilisation activity balance of the E-mMWCNT preparation*

Fraction	Symbol	Reducing sugar (g L^{-1})	Reaction rate (g L^{-1} min^{-1})	Activity (U)
Enzyme stock offered to support	A_i	4.6	0.92	256
Residual supernatant after coupling	A_r	0.9	0.18	50
Recovered E-*m*MWCNT preparation	E_a	1.8	0.36 (0.25 – 0.46)	100
Immobilisation yield	$(A_i - A_r)/A_i \cdot 100$	–	80 %	–
Loss of activity upon immobilisation	$(A_i - A_r - E_a)/A_i \cdot 100$	–	41 %	–
Activity yield	$E_a/(A_i - A_r) \cdot 100$	–	48 %	–
Activity recovery	$E_a/A_i \cdot 100$	–	39 %	–
Specific activity at 0.1 g loading	–	–	1000 U g^{-1}	–

Each rate determined by DNS assay on CMC in triplicate using a 5-min incubation in a 50-mL reaction volume; activity in units (U), one unit releasing 1 μmol glucose equivalents per minute.

The undiluted free enzyme concentrate has a specific activity of approximately 1070 U g^{-1} for comparison. A_r measures activity still detectable in the supernatant, so $A_i - A_r$ does not, by itself, separate activity bound to the support from activity inactivated in solution during coupling.

was a potential indicator that the immobilised catalyst possibly suffered external transport limitation. Furthermore, the absence of a further increase in yield above 200 rpm suggests that the remaining transport limitation may reside within the nanotube network in addition to the external film.

Immobilisation activity efficiency

The initial free enzyme amount offered to the support released 4.6 g L^{-1} reducing sugar, corresponding to a reaction rate of 0.92 g L^{-1} min^{-1} and an activity of 256 U (Table 1). The residual supernatant after enzyme coupling released 0.9 g L^{-1} at 0.18 g L^{-1} min^{-1}, equivalent to 50 U. The recovered E-*m*MWCNT preparation released 1.8 g L^{-1} at 0.36 g L^{-1} min^{-1}, equivalent to 100 U. The activity balance therefore corresponded to an immobilisation yield of 80 %, a loss of 41 % of the activity offered, an activity yield of 48 % of the activity removed from solution, and an activity recovery of 39 % of the activity initially offered. Based on the offered activity, 20 % remained detectable in the supernatant, 41 % was lost, and 39 % was recovered in catalytically active form on the support. The latter two fractions together accounted for the 80 % enzyme activity removed from solution. The preparation had a specific activity of 1000 U per gram at the 0.1 g loading used throughout the study compared with approximately 1070 U per gram for the undiluted free enzyme concentrate.

A loss of this magnitude is expected for covalent attachment through a bifunctional cross-linker, in which some of the bound molecules are routinely inactivated by non-productive orientation, multipoint attachment, or distortion of the active site. No support-free control was performed.

Effect of glutaraldehyde concentration and operational reuse

Glutaraldehyde concentration was screened over the range 7.5–17.5 % (v/v), with each preparation subjected to twelve consecutive reaction cycles using 5 g L^{-1} CMC (Table 2, Fig. 6). Glutaraldehyde concentration had a much greater effect on operational longevity than on first-cycle activity. At 7.5 % (v/v), the preparation was essentially inactive, yielding 0.3 ± 0.0 g L^{-1} in the first cycle and no detectable product beyond the second, suggesting too few covalent linkages were formed to retain the enzyme. The highest first-cycle yields were obtained at 15 % (v/v) and 17.5 % (v/v), at 4.9 ± 0.2 and 3.2 ± 0.2 g L^{-1} respectively; however, neither preparation held on to them. The 15 % (v/v) preparation declined from 2.9 g L^{-1} at the fourth cycle to 1.5 g L^{-1} at the fifth and became undetectable from the ninth cycle onwards. The 17.5 % (v/v) preparation declined more gradually and remained measurable to the ninth cycle, although not monotonically, with increases at the fifth and ninth cycles before activity was lost from the tenth cycle onwards. At 12.5 % (v/v), the first-cycle yield of 2.7 ± 0.1 g L^{-1} exceeded that of the 10 % (v/v) preparation, but activity was completely lost after the fifth cycle.

The preparation cross-linked with 10.0 % (v/v) glutaraldehyde gave a more modest first-cycle yield of 2.2 ± 0.2 g L^{-1} but was the only one to sustain activity throughout all twelve cycles. Yield was retained at 91 % of the first-cycle value by the fifth cycle and 55 % by the eighth cycle and remained measurable at the twelfth (0.6 g L^{-1}), corresponding to an overall decline of 73 % across the cycle. The cumulative yield over the twelve cycles was 17.6 g L^{-1}, equivalent to eight first-cycle batches from a

Table 2 – *Reducing sugar yield by glutaraldehyde concentration over twelve consecutive reuse cycles (mean ± SD, n = 3)*

Cycle	Glutaraldehyde 7.5 % (v/v)	Glutaraldehyde 10.0 % (v/v)	Glutaraldehyde 12.5 % (v/v)	Glutaraldehyde 15.0 % (v/v)	Glutaraldehyde 17.5 % (v/v)
1	0.3 ± 0.0	2.2 ± 0.2	2.7 ± 0.1	4.9 ± 0.2	3.2 ± 0.2
2	0.1 ± 0.0	2.4 ± 0.1	1.3 ± 0.1	3.3 ± 0.2	2.1 ± 0.1
3	n.d.	2.2 ± 0.1	1.1 ± 0.1	3.3 ± 0.1	2.0 ± 0.1
4	n.d.	2.0 ± 0.1	0.9 ± 0.0	2.9 ± 0.0	1.4 ± 0.1
5	n.d.	2.0 ± 0.1	0.9 ± 0.1	1.5 ± 0.0	1.8 ± 0.1
6	n.d.	1.4 ± 0.0	n.d.	1.2 ± 0.2	1.5 ± 0.1
7	n.d.	1.2 ± 0.0	n.d.	1.1 ± 0.1	0.9 ± 0.1
8	n.d.	1.2 ± 0.0	n.d.	0.6 ± 0.0	0.8 ± 0.1
9	n.d.	0.9 ± 0.0	n.d.	n.d.	1.1 ± 0.0
10	n.d.	0.8 ± 0.0	n.d.	n.d.	n.d.
11	n.d.	0.7 ± 0.0	n.d.	n.d.	n.d.
12	n.d.	0.6 ± 0.0	n.d.	n.d.	n.d.

Assay conditions: 5 g L^{-1} CMC, pH 4.0, 55 °C, 200 rpm; magnetic recovery and washing between cycles. n.d. = not detected.

Derived from the twelve-cycle series (v/v)

Derived quantity	7.5 %	10.0 %	12.5 %	15.0 %	17.5 %
Cumulative yield (g L^{-1})	0.4	17.6	6.9	18.8	14.8
First-cycle batch equivalents	1.3	8.0	2.6	3.8	4.6
Retention at cycle 5 (%)	n.d.	91	33	31	56
Retention at cycle 8 (%)	n.d.	55	n.d.	12	25
Last active cycle	2	12	5	8	9

Cumulative yield is summed over the twelve cycles. Retention is expressed as a percentage of each preparation's own first-cycle yield. First-cycle batch equivalents = cumulative yield ÷ first-cycle yield. Last active cycle is the final cycle at which reducing sugar was detected.

The 10.0 % (v/v) preparation was selected for all subsequent work based on expressed activity per unit of immobilised activity. One-way ANOVA on first-cycle yields: $F(4, 10) = 478$, $p < 0.001$; Tukey's HSD test separated every pair of concentrations.

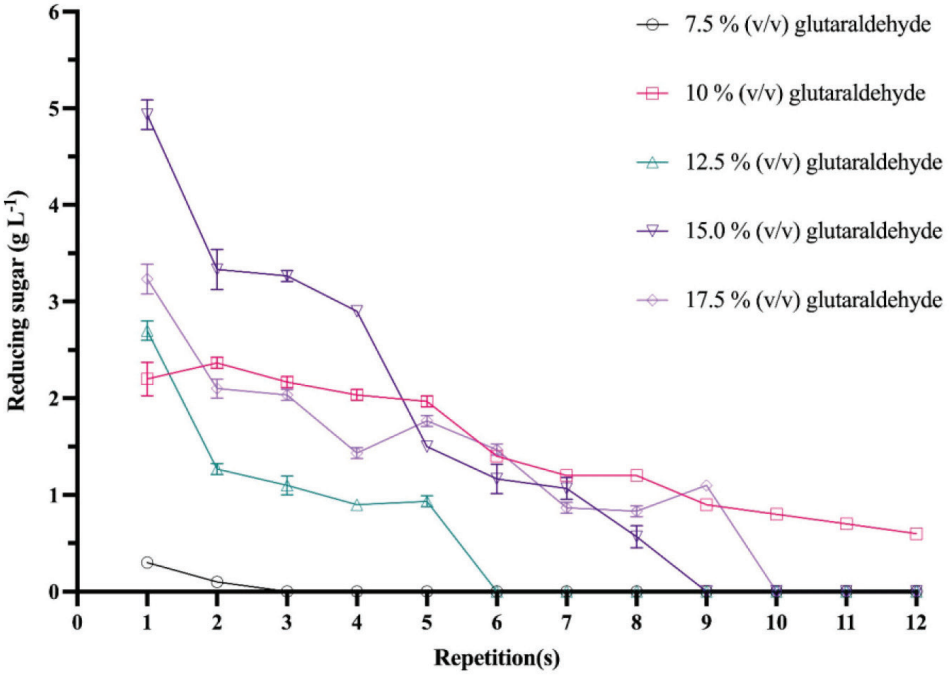


Fig. 6 – *Reducing sugar yield over twelve consecutive reaction cycles for preparations cross-linked with 7.5–17.5 % (v/v) glutaraldehyde, using 5 g L^{-1} CMC as substrate*

single enzyme charge. This concentration was selected on the basis of operational durability per unit of immobilised activity rather than absolute output. The cumulative yield of the 10 % (v/v) preparation was 8.0 times its own first-cycle yield, compared with 3.8 for the 15 % (v/v) preparation and 4.6 for the 17.5 % (v/v) preparation. Moreover, the 10 % (v/v) preparation retained more than half of its first-cycle activity to the eighth cycle, by which point the 15 % (v/v) preparation had declined to 12 % of its own first-cycle value. The nearest competitor was arguably the 17.5 % (v/v) preparation rather than the 15 % (v/v) preparation. It started higher, at 3.2 ± 0.2 versus 2.2 ± 0.2 g L^{-1}, and remained measurable to the ninth cycle, giving a cumulative yield of 14.8 g L^{-1}, or 4.6 first-cycle equivalents. However, in terms of durability per unit of immobilised activity, it fell short of the 10 % (v/v) preparation: it retained 56 % of its own first-cycle yield at the fifth cycle and 25 % at the eighth, compared with 91 % and 55 %, respectively, for the 10 % (v/v) preparation. It also delivered a lower cumulative yield, 14.8 versus 17.6 g L^{-1}, despite its higher initial charge, and lost detectable activity three cycles earlier. The differences in absolute yield at the fifth and eighth cycles were significant (Tukey's HSD, $p < 0.05$). At the sixth and ninth cycles, the 17.5 % (v/v) preparation was marginally higher than the 10 % (v/v) preparation. The preferential selection for 10 % (v/v) therefore rests on cumulative output, mid-series retention and operational lifetime rather than on outperforming the 17.5 % (v/v) preparation at every individual cycle. The 15 % (v/v) preparation did deliver a marginally higher absolute cumulative yield, 18.8 g L^{-1} over eight cycles versus 17.6 g L^{-1} over twelve for the 10 % (v/v) preparation, but it did so by providing a higher initial activity that it could not sustain. Its output had declined substantially well before the complete cycle ended. ANOVA of the first-cycle yields confirmed a significant effect of glutaraldehyde concentration on reducing sugar yield, $F(4, 10) = 478$, $p < 0.001$, and Tukey's HSD test separated every pair of concentrations. When the analysis was repeated cycle-by-cycle, the 10 % (v/v) preparation was significantly lower than the 12.5, 15, and 17.5 % (v/v) preparations at the first cycle, and significantly higher than all four other concentrations at the fifth and eighth cycles.

Since the purpose of immobilisation was repeated use rather than peak single-cycle activity, 10.0 % (v/v) was selected for all subsequent work. The loss of longevity at higher concentrations may be attributable to excessive cross-linking, which stiffens the enzyme preparation and makes it harder to wash product and residual substrate between cycles. Magnetic recovery was rapid and visually complete at every cycle, requiring neither filtration nor centrifugation. Whether the gentle handling enabled by magnetic recovery contributed to the observed activity retention was not tested, as no filtration-recovered control was included. The gradual decline in activity probably reflects a combination of progressive inactivation of active sites and loss of incompletely cross-linked molecules during repeated washing. These two contributions cannot be distinguished without a dedicated leaching study.

Kinetic evaluation using CMC as substrate

The kinetic behaviour of E-*m*MWCNT was evaluated using CMC as the substrate and compared with the free enzyme preparation, with each preparation tested under its own optimised conditions. Both profiles showed saturation kinetics, with velocity increasing with substrate concentration until saturation level was approached. For the immobilised preparation, the Michaelis–Menten parameters are apparent, lumped values. Both free and immobilised preparations contained 100 U of activity.

For the free enzyme, nonlinear fitting gave a V_{max} of 2.22 g L^{-1} min^{-1} and a K_m of 12.9 g L^{-1} (R^2 = 0.99). The nonlinear plot is shown in Fig. 7(a), with the saturation level approached at approximately 15 g L^{-1} substrate. In contrast, the E-*m*MWCNT preparation approached saturation only at higher substrate concentrations, at 20 g L^{-1} (Fig. 7(b)). Nonlinear fitting of the immobilised system gave an apparent V_{max} of 0.36 g L^{-1} min^{-1} and an apparent K_m of 17.2 g L^{-1} (R^2 = 0.97). The free enzyme preparation exhibited a higher V_{max} and lower K_m than E-*m*MWCNT.

The K_m/V_{max} ratio increased from approximately 6 min for the free enzyme to approximately 48 min for E-*m*MWCNT, so the immobilised preparation took roughly eight times longer to hydrolyse the same amount of CMC in a single pass.

The lower apparent V_{max} and higher apparent K_m of E-*m*MWCNT preparation indicated that substrate accessibility to the enzyme active sites was affected following immobilisation, possibly due to partial occlusion of active sites, steric hindrance, and mass transfer limitations. These effects may become more pronounced at higher CMC concentrations because increasing substrate concentration also increases solution viscosity and can reduce substrate diffusion. The reaction velocity of E-*m*MWCNT decreased above 25 g L^{-1} CMC, with V_0 falling from 0.20 to 0.16 g L^{-1} min^{-1} at 30 g L^{-1}, consistent with mass transfer resistance associated with higher viscosity at high substrate loading. Compared with previously reported immobilised cellulase systems[25,26], the retention measured here is competitive with other immobilised cellulase systems assayed using the same substrate. Two studies allow a direct comparison because both investigated

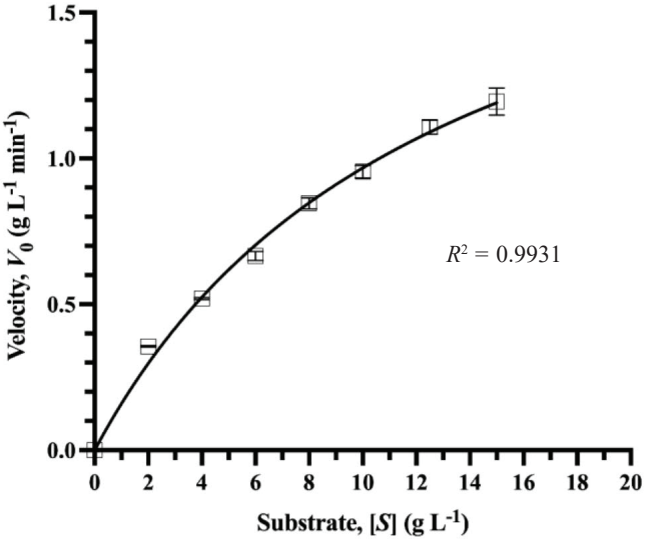


Fig. 7(a) – *Nonlinear plot of free enzyme with CMC as substrate*

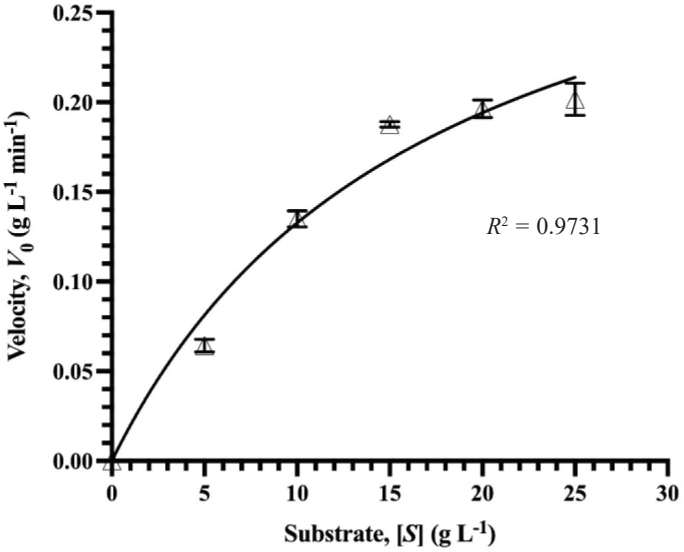


Fig. 7(b) – *Nonlinear plot of E-mMWCNT with CMC as substrate*

repeated use with carboxymethyl cellulose where cellulase coupled through glutaraldehyde to zinc-doped magnetic nanoparticles retained 50 % of its initial activity after five cycles[27], whereas cellulase adsorbed onto multi-walled carbon nanotubes and subsequently encapsulated in calcium alginate retained 71.5 % after seven cycles[28], versus 55 % after eight cycles in this present study, which remained measurable through twelve cycles. Therefore, the preparation described here outlasted the glutaraldehyde-coupled zinc-doped magnetic support, whereas the alginate-encapsulated composite showed greater activity retention but relied on a material that could not be recovered magnetically and required filtration. Nonetheless, enzyme loading, cycle duration, and the definition of a completed cycle differ among the three studies, so these figures are indicative only. On the kinetic side, the observed 8.2-fold increase in K_m/V_{max} falls between the 2.5-fold increase reported for cellulase immobilised on chitosan-modified magnetic biochar[29] and the 16.4-fold increase reported for cellulase immobilised on multi-walled carbon nanotubes[30], both assayed on carboxymethyl cellulose. The latter increase was likewise attributed to diffusional restriction within the support.

Evidence of diffusion limitation in the E-*m*MWCNT preparation is provided by the double-reciprocal plots for both free and immobilised enzyme preparations (Fig. 8). The free enzyme produced the usual straight line over the range of substrate concentrations studied, whereas the E-*m*MWCNT plot is convex towards the 1/*S*-axis across the range tested, consistent with an immobilised catalyst subject to mass transfer limitation. Application of equation (4) gave an effective liquid–solid volumetric mass-transfer coefficient of 0.016 min^{-1} for CMC under the present conditions.

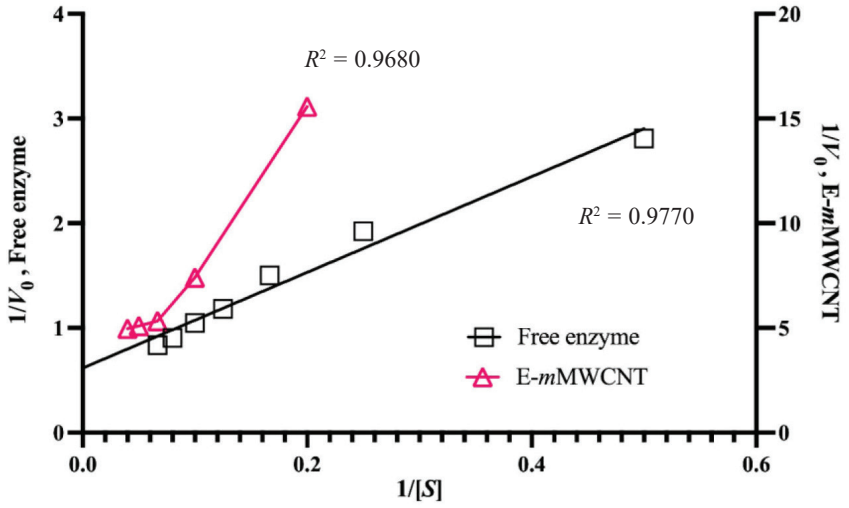


Fig. 8 – *Double-reciprocal plot of the free enzyme and E-mMWCNT with CMC as substrate*

Table 3 – *Kinetic parameters of the free enzyme and E-mMWCNT preparations using CMC as substrate*

Parameter	Free enzyme	E-*m*MWCNT
V_{max} (g L^{-1} min^{-1})	2.22 (2.00 – 2.48)	0.36 (0.30 – 0.46)[a]
K_m (g L^{-1})	12.9 (10.7 – 15.7)	17.2 (11.6 – 26.8)[a]
K_m/V_{max} (min)	5.8	47.8
Substrate range fitted (g L^{-1})	2 – 15	5 – 25
R^2 of nonlinear fit	0.99	0.97

[a]Apparent values. They are obtained from the observed rates of a suspended catalyst and therefore carry the external transport resistance; the free-enzyme constants are intrinsic.
Values in parentheses are the 95 % confidence intervals returned by the nonlinear fit. Both preparations contained 100 U of activity, each assayed under their respective optimised conditions. The effective liquid–solid volumetric mass-transfer coefficient k_La is 0.016 min^{-1} from the difference of the two double-reciprocal slopes.

Advantages and limitations of the E-*m*MWCNT preparation

The data support two clear operational benefits: (i) saturation magnetisation increased from 6.95 to 46.7 emu g^{-1}, with remanence of 2.02 emu g^{-1} and coercivity of 2.07 G, indicating soft-magnetic behaviour, which allowed rapid recovery using an external magnet without filtration or centrifugation; and (ii) the preparation sustained twelve consecutive reaction cycles, delivering a cumulative output equivalent to eight first-cycle batches from a single enzyme charge.

Against these advantages, the preparation incurred a clear single-pass kinetic penalty, where catalytic efficiency on CMC was approximately eightfold lower than that of the free enzyme. The analysis attributed this decrease primarily to external and internal transport limitations. The trade-off is therefore between single-pass rate and cumulative output per enzyme charge, and based on the present data, the latter favours immobilisation.

Several limitations should be noted. All catalytic measurements used CMC, a soluble model substrate for endoglucanase activity rather than a proxy for lignocellulose, and performance on insoluble or native cellulosic substrates cannot be extrapolated from these data. Hydrolysis of insoluble cellulose requires productive enzyme adsorption onto the substrate surface, which a covalently tethered enzyme within an entangled network may not achieve in the same manner. Moreover, the cocktail components most relevant to such substrates, namely cellobiohydrolases acting processively from chain ends and AA9 acting on crystalline regions, were not characterised after immobilisation in this study.

The immobilisation in this study was characterised on an activity basis rather than a protein basis because the absolute protein portion of the individual cocktail components could not be resolved. Instead, component-specific assays would be required to characterise the immobilisation of individual activities, e.g., *p*-nitrophenyl-β-D-glucopyranoside for β-glucosidase, xylan with DNS detection for hemicellulase activity, and an Amplex Red or H_2O_2-consumption assay with an added electron donor for AA9. No dedicated leaching experiment was conducted under reaction conditions with continuous agitation; therefore, leaching during operation cannot be distinguished from active-site inactivation as a cause of activity decline across cycles. Thermal and storage stability were not determined in this study. The repeated-use investigation establishes operational durability across reaction cycles but not resistance to thermal or storage inactivation in isolation. Formal pre-incubation and storage trials would be required to establish an operational half-life. In this study, FESEM analysis was qualitative; nanotube diameter distribution, iron oxide particle size, and coating thickness were not determined, and the nanotube outer diameter reported here is based on the supplier's specification. Finally, the CMC assays were performed without a buffering system, so pH drift during the reaction cannot be excluded and may have contributed to the steep loss of activity observed, particularly at pH 5.0.

Conclusion

A magnetically recoverable enzyme-immobilised MWCNT composite (E-*m*MWCNT) was prepared by acid oxidation of pristine MWCNTs, Fe_3O_4 deposition, AEAPTMS silanisation, glutaraldehyde activation, and covalent immobilisation of the NS22257 enzyme cocktail. The composite was evaluated by reaction optimisation, kinetic evaluation, and a twelve-cycle reuse study using CMC as substrate. Three main implications follow from the findings: Glutaraldehyde concentration had a substantially greater effect on operational longevity than on first-cycle activity. The 10.0 % (v/v) preparation gave a more modest first-cycle yield, yet it delivered 8.0 first-cycle batch equivalents versus 4.6 and 3.8 for the 17.5 % (v/v) and 15 % (v/v)

preparations, respectively, and was the only preparation to sustain activity across all twelve cycles. The kinetic penalty cannot be attributed to bulk diffusion alone.

The resistances-in-series treatment quantified the external transport contribution as an effective liquid–solid volumetric mass-transfer coefficient of 0.016 min^{-1}. However, internal transport within the nanotube network, and factors associated with enzyme immobilisation, including enzyme orientation, multipoint attachment, and competition among cocktail components for a limited number of activated aldehyde sites, still present a gap. The 8.2-fold increase in K_m/V_{max} is the offset for repeated operational use of a single enzyme charge while a free-enzyme charge is not recoverable at all. The resulting trade-off is between single-pass rate and cumulative output per enzyme charge. Based on the present results, E-*m*MWCNT is suitable for applications in which catalyst recovery defines the process. However, these findings characterise endoglucanase activity using CMC as a soluble model substrate. The performance of E-*m*MWCNT on insoluble lignocellulosic feedstocks remains to be established.

SUPPLEMENTARY MATERIALS

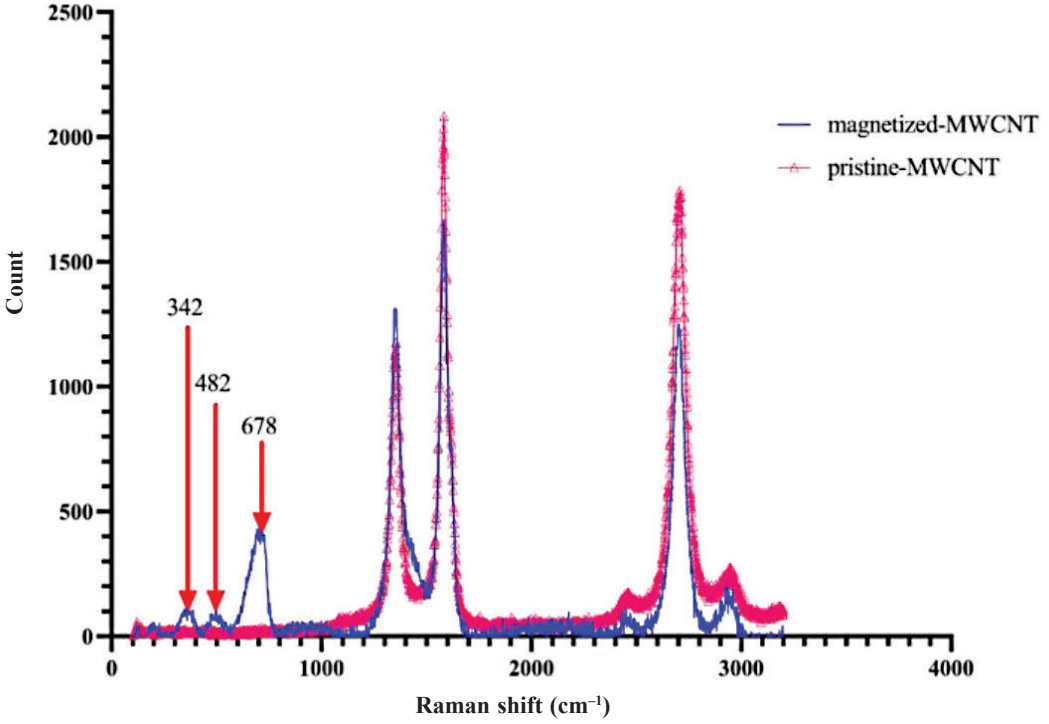


Fig. S1 – *Raman spectra for pristine MWCNT and E-mMWCNT samples*

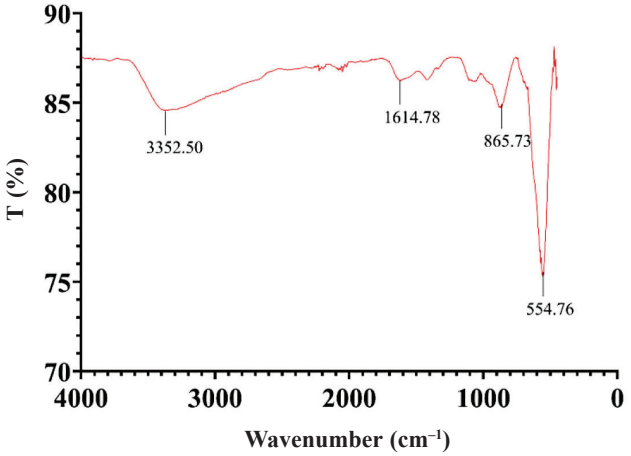


Fig. S2 – *FTIR spectrum of carboxylated-mMWCNT samples*

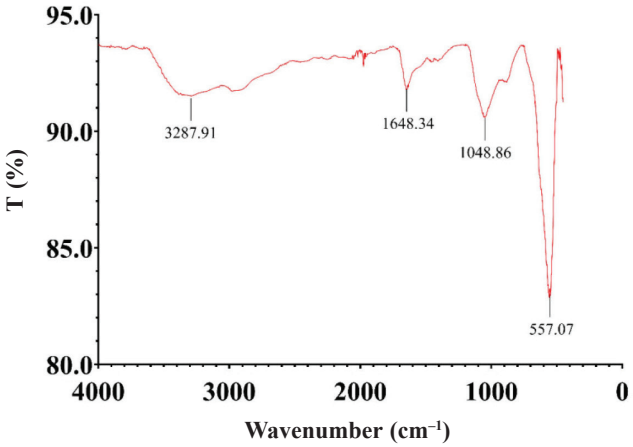


Fig. S3 – *FTIR spectrum of carboxylated-mMWCNT samples with AEAPTMS functionalisation*

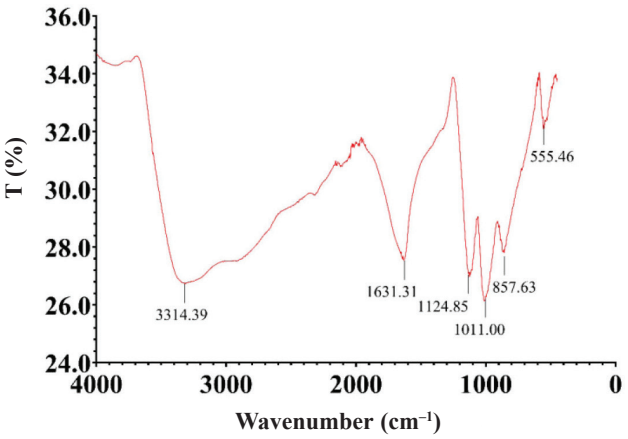


Fig. S4 – *FTIR spectrum of carboxylated-mMWCNT samples with AEAPTMS and glutaraldehyde cross-linking*

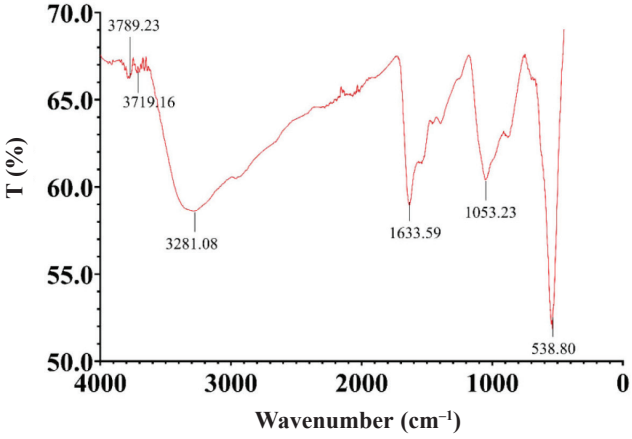


Fig. S5 – *FTIR spectrum of E-mMWCNT samples*

Spectra were recorded on a Perkin Elmer Spectrum 400 spectrometer with a diamond ATR accessory, solid samples, 4000–450 cm^{-1} against a background spectrum. *m*MWCNT represents acid-oxidised, magnetised MWCNTs. n.d.: no peak reported at that stage.

Three further labels returned for the E-*m*MWCNT spectrum at 3789.23, 3719.16 and 3663.51 cm^{-1} lie in a region where the trace is visibly noisy and are not assigned.

The band near 1630 cm^{-1} is reported at every stage from glutaraldehyde activation onward and is of comparable magnitude to the glutaraldehyde-activated support and in E-*m*MWCNT. It therefore cannot be assigned to the enzyme amide I vibration on position alone: the imine formed between glutaraldehyde and the AEAPTMS amine absorbs in the same region. No amide II band was reported in any spectrum.

Table S1 – *FTIR peak assignments for MWCNTs at each stage of modification*

Assignment	*c*-*m*MWCNT (Fig. S2)	AEAPTMS-silanised (Fig. S3)	Glutaraldehyde-activated (Fig. S4)	E-*m*MWCNT (Fig. S5)
O–H/N–H stretching	3352.50	3287.91	3314.39	3281.08
C=C skeletal (*c*-*m*MWCNT); N–H bending, C=N (imine) and amide I at the later stages	1614.78	1648.34	1631.31	1633.59
Si–O–Si/Si–O–C/C–O stretching	n.d.	1048.86	1124.85, 1011.00	1053.23
Out-of-plane/Si–O bending	865.73	n.d.	857.63	n.d.
Fe–O stretching (iron oxide)	554.76	557.07	555.46	538.80

List of symbols

D – Raman *D*-band (disordered/defect-induced carbon mode), –

G – Raman *G*-band (graphitic in-plane stretching mode), –

K_m – Michaelis constant, g L^{-1}

k_La – effective liquid–solid volumetric mass-transfer coefficient (lumped), min^{-1}

$[S]$ – substrate concentration (CMC), g L^{-1}

°C – temperature, Celsius

V_0 – initial reaction velocity, g L^{-1} min^{-1}

V_{max} – maximum reaction velocity, g L^{-1} min^{-1}

V_{max}/K_m – apparent first-order rate constant, min^{-1}

v – reaction velocity (Eqs. 1–3), g L^{-1} min^{-1}

A_i – activity offered to the support, U

A_r – activity remaining in the supernatant after coupling, U

E_a – activity recovered on the support, U

U – enzyme activity unit; 1 µmol glucose equivalents released per minute, –

k_L – liquid-film mass-transfer coefficient, m min^{-1}

a – specific interfacial area, m^{-1}

References

1. *Bié, J., Sepodes, B., Fernandes, P. C. B., Ribeiro, M. H. L.,* Enzyme immobilization and co-immobilization: Main framework, advances and some applications, Processes **10** (2022) 494. doi: https://doi.org/10.3390/pr10030494
2. *Liu, D. M., Dong, C.*, Recent advances in nano-carrier immobilized enzymes and their applications, Process Biochem. **92** (2020) 464. doi: https://doi.org/10.1016/j.procbio.2020.02.005
3. *Kumari, A., Rajeev, R., Benny, L., Sudhakar, Y. N., Varghese, A., Hegde, G.*, Recent advances in carbon nanotubes-based biocatalysts and their applications, Adv. Colloid Interface Sci. **297** (2021) 102542. doi: https://doi.org/10.1016/j.cis.2021.102542
4. *Kumar, S., Sidhu, H. K., Paul, A. K., Bhardwaj, N., Thakur, N. S., Deep, A.,* Bioengineered multi-walled carbon nanotube (MWCNT) based biosensors and applications thereof, Sens. Diagn. **2** (2023) 1390. doi: https://doi.org/10.1039/d3sd00176h
5. *Gama Cavalcante, A. L., Dari, D. N., Izaias da Silva Aires, F., Carlos de Castro, E., Moreira dos Santos, K., Sousa dos Santos, J. C.,* Advancements in enzyme immobilization on magnetic nanomaterials: Toward sustainable industrial applications, RSC Adv. **14** (2024) 17946. doi: https://doi.org/10.1039/d4ra02939a
6. *Kaur, P., Jana, A. K.,* Amino functionalization of magnetic multiwalled carbon nanotubes with flexible hydrophobic spacer for immobilization of *Candida rugosa* lipase and application in biocatalytic production of fruit flavour esters ethyl butyrate and butyl butyrate, Appl. Nanosci. **13** (2023) 4291. doi: https://doi.org/10.1007/s13204-022-02657-6
7. *Yasmin, H. A. N., Naresh, S., Kunasundari, B., Shuit, S. H.,* Immobilization of cellulase on magnetized multiwall carbon nanotubes (m-MWCNTs) synthesized via eco-friendly (water-based) method, Chem. Pap. **76** (2022) 453. doi: https://doi.org/10.1007/s11696-021-01874-7
8. *Runprapan, N., Kao, P. Y., Liu, C. T., Peng, J. C., Wang, F. M., Yuan, C. C.,* A comparative study of MWCNTs-based antibody immobilization strategies for enhanced electrochemical CA125 detection, J. Taiwan Inst. Chem. Eng. **184** (2026) 106253. doi: https://doi.org/10.1016/j.jtice.2025.106253
9. *Johnsen, H. R., Krause, K.,* Cellulase activity screening using pure carboxymethylcellulose: application to soluble cellulolytic samples and to plant tissue prints, Int. J. Mol. Sci. **15** (2014) 830. doi: https://doi.org/10.3390/ijms15010830
10. *Atieh, M. A., Bakather, O. Y., Al-Tawbini, B., Bukhari, A. A., Abuilaiwi, F. A., Fettouhi, M. B.,* Effect of carboxylic functional group functionalized on carbon nanotubes surface on the removal of lead from water, Bioinorg. Chem. Appl. **2010** (2010) 603978. doi: https://doi.org/10.1155/2010/603978
11. *Bikiaris, D., Vassiliou, A., Chrissafis, K., Paraskevopoulos, K. M., Jannakoudakis, A., Docoslis, A.,* Effect of acid treated multi-walled carbon nanotubes on the mechanical, permeability, thermal properties and thermo-oxidative stability of isotactic polypropylene, Polym. Degrad. Stab. **93** (2008) 952. doi: https://doi.org/10.1016/j.polymdegradstab.2008.01.033
12. *Wepasnick, K. A., Smith, B. A., Schrote, K. E., Wilson, H. K., Diegelmann, S. R., Fairbrother, D. H.,* Surface and structural characterization of multi-walled carbon nanotubes following different oxidative treatments, Carbon **49** (2011) 24. doi: https://doi.org/10.1016/j.carbon.2010.08.034
13. *Ba-Abbad, M. M., Benamour, A., Ewis, D., Mohammad, A. W., Mahmoudi, E.,* Synthesis of Fe_3O_4 nanoparticles with different shapes through a co-precipitation method and their application, JOM **74** (2022) 3531. doi: https://doi.org/10.1007/s11837-022-05380-3
14. *Huaccallo, Y., Álvarez-Torrellas, S., Marín, M. P., Gil, M. V., Larriba, M., Águeda, V. I., Ovejero, G., García, J.,* Magnetic Fe_3O_4/multi-walled carbon nanotubes materials for a highly efficient depletion of diclofenac by catalytic wet peroxide oxidation, Environ. Sci. Pollut. Res. **26** (2019) 22372. doi: https://doi.org/10.1007/s11356-019-05597-x
15. *Kulpa-Greszta, M., Tomaszewska, A., Michalicha, A., Sikora, D., Dziedzic, A., Wojnarowska-Nowak, R., Belcarz, A., Pązik, R.,* Alternating magnetic field and NIR energy conversion on magneto-plasmonic Fe_3O_4@APTES–Ag heterostructures with SERS detection capability and antimicrobial activity, RSC Adv. **12** (2022) 27396. doi: https://doi.org/10.1039/d2ra05207e
16. *De Melo, R. R., Alnoch, R. C., Vilela, A. F. L., De Souza, E. M., Krieger, N., Ruller, R., Sato, H. H., Mateo, C.,* New heterofunctional supports based on glutaraldehyde-activation: a tool for enzyme immobilization at neutral pH, Molecules **22** (2017) 1088. doi: https://doi.org/10.3390/molecules22071088
17. *Miller, G. L.,* Use of dinitrosalicylic acid reagent for determination of reducing sugar, Anal. Chem. **31** (1959) 426. doi: https://doi.org/10.1021/ac60147a030
18. *Horvath, C., Engasser, J.-M.,* External and internal diffusion in heterogeneous enzyme systems, Biotechnol. Bioeng. **16** (1974) 909. doi: https://doi.org/10.1002/bit.260160705
19. *Lilly, M. D., Hornby, W. E., Crook, E. M.,* The kinetics of carboxymethylcellulose-ficin in packed beds, Biochem. J. **100** (1966) 718. doi: https://doi.org/10.1042/bj1000718
20. *Jubb, A. M., Allen, H. C.,* Vibrational spectroscopic characterization of hematite, maghemite, and magnetite thin films produced by vapor deposition, ACS Appl. Mater. Interfaces **2** (2010) 2804. doi: https://doi.org/10.1021/am1004943
21. *Baabu, P. R. S., Kumar, H. K., Gumpu, M. B., Babu K, J., Kulandaisamy, A. J., Rayappan, J. B. B.,* Iron oxide nanoparticles: A review on the province of its compounds, properties and biological applications, Materials **16** (2023) 59. doi: https://doi.org/10.3390/ma16010059
22. *Gabelica, I., Ćurković, L., Mandić, V., Panžić, I., Ljubas, D., Zadro, K.,* Rapid microwave-assisted synthesis of $Fe_3O_4/SiO_2/TiO_2$ core-2-layer-shell nanocomposite for photocatalytic degradation of ciprofloxacin, Catalysts **11** (2021) 1136. doi: https://doi.org/10.3390/catal11101136
23. *Guzik, U., Hupert-Kocurek, K., Wojcieszynska, D.,* Immobilization as a strategy for improving enzyme properties—application to oxidoreductases, Molecules **19** (2014) 8995. doi: https://doi.org/10.3390/molecules19078995
24. *Homaei, A. A., Sariri, R., Vianello, F., Stevanato, R.,* Enzyme immobilization: An update, J. Chem. Biol. **6** (2013) 185. doi: https://doi.org/10.1007/s12154-013-0102-9
25. *Kotwal, N., Pathania, D., Singh, A., Sheikh, Z. U. D., Kothari, R.,* Enzyme immobilization with nanomaterials for hydrolysis of lignocellulosic biomass: Challenges and future perspectives, Carbohydr. Res. **543** (2024) 109208. doi: https://doi.org/10.1016/j.carres.2024.109208

26. *Rajnish, K. N., Samuel, M. S., John J, A., Datta, S., Chandrasekar, N., Balaji, R., Jose, S., Selvarajan, E.,* Immobilization of cellulase enzymes on nano and micro-materials for breakdown of cellulose for biofuel production — a narrative review, Int. J. Biol. Macromol. **182** (2021) 1793. doi: https://doi.org/10.1016/j.ijbiomac.2021.05.176
27. *Abraham, R. E., Verma, M. L., Barrow, C. J., Puri, M.,* Suitability of magnetic nanoparticle immobilised cellulases in enhancing enzymatic saccharification of pretreated hemp biomass, Biotechnol. Biofuels **7** (2014) 90. doi: https://doi.org/10.1186/1754-6834-7-90
28. *Li, L. J., Xia, W. J., Ma, G. P., Chen, Y. L., Ma, Y. Y.,* A study on the enzymatic properties and reuse of cellulase immobilized with carbon nanotubes and sodium alginate, AMB Express **9** (2019) 112. doi: https://doi.org/10.1186/s13568-019-0835-0
29. *Mo, H., Qiu, J.,* Preparation of chitosan/magnetic porous biochar as support for cellulase immobilization by using glutaraldehyde, Polymers **12** (2020) 2672. doi: https://doi.org/10.3390/polym12112672
30. *Azmi, N. D., Saat, M. N., Mohamad Annuar, M. S.,* Kinetic hydrolysis of cellulose biopolymer by carbon nanotubes immobilized cellulase, J. Adv. Res. Appl. Sci. Eng. Technol. **30** (2023) 325. doi: https://doi.org/10.37934/araset.30.3.325333